Tuijin Jishu/Journal of Propulsion Technology
ISSN: 1001-4055
Vol. 46 No. 1 (2025)

Numerical Investigation of Inlet Velocity and Aspect Ratio Effects on Heat Transfer and Pressure Losses in Regenerative Cooling Channels

Nabila Alili[1], Mohammed Amine Djeffal[2], Ali Benouar[3], Nabil Benamara[2], Khacem Kaddouri[1], Mokadem Salem[1],

[1] *Mechanical Engineering Department, Djillali Liabes University, Laboratory of physical mechanics of materials (LMPM), Sidi Bel Abbes, Algeria.*

[2] *Mechanical Engineering Department, Djillali Liabes University, Laboratory of materials and reactive Systems (LMSR), Sidi Bel Abbes, Algeria.*

[3] *Higher School of Electrical and Energy Engineering ESGEE, Laboratory of complex reactive Systems (LCS), Oran, Algeria.*

Abstract: - This study investigates the effect of channel aspect ratio and inlet velocity on heat transfer and pressure losses in rectangular channels cooled by forced convection using methane as a coolant. The study employs a copper alloy channel with three configurations: Rec-1 (aspect ratio < 1), Rec-2 (aspect ratio = 1), and Rec-3 (aspect ratio > 1). Numerical simulations using ANSYS Fluent 18.1 revealed that increasing inlet velocity significantly enhances heat transfer, with a 118% difference in heated wall temperature T_{wg} between 5 m/s and 15 m/s, but also causes a substantial rise in pressure losses (240%). Aspect ratio modifications demonstrate distinct advantages: Rec-1 minimizes external wall temperature T_{wa}, crucial for composite materials; Rec-2 achieves the lowest pressure losses; and Rec-3 reduces T_{wg} without a significant increase in pressure losses. These findings provide valuable insights into optimizing regenerative cooling systems in rocket engines by balancing thermal performance and hydraulic losses.

Keywords*:* Regenerative Cooling, Rectangular channels, Aspect Ratio, Heat Transfer, Pressure Losses.

1. Introduction

Next-generation rocket engines are pushing the boundaries of performance, requiring innovative solutions, as highlighted by several recent studies [1-6], particularly in the field of cooling [7,8]. Regenerative cooling, where the fuel (typically) absorbs heat before combustion, is an essential and effective cooling technique for liquid propellant rocket engines (LPRE) with high thrust and long combustion durations.

Early engines, such as the V2 and its derivatives, used double-wall chambers. However, as engines became increasingly efficient and required even higher pressures, wall designs evolved. Tubular and later rectangular channels became the most common construction type [9].

The choice of fuel also plays a critical role in engine performance and cooling efficiency. Recently, methane has emerged as a promising fuel due to its advantageous balance of thermodynamic properties [10-12]. In regenerative cooling systems, methane flows at a pressure above its critical pressure. As it passes through the cooling channels, its temperature increases without a phase transition but shifts from a liquid-like state to a gas-like state at a temperature known as the pseudo-critical temperature. At this temperature, its properties, such as specific heat, change drastically. As shown in Fig. 1, taken from the NIST database [13] the specific heat reaches a peak around 214 K (pseudo-critical temperature), at a pressure of 9 MPa.

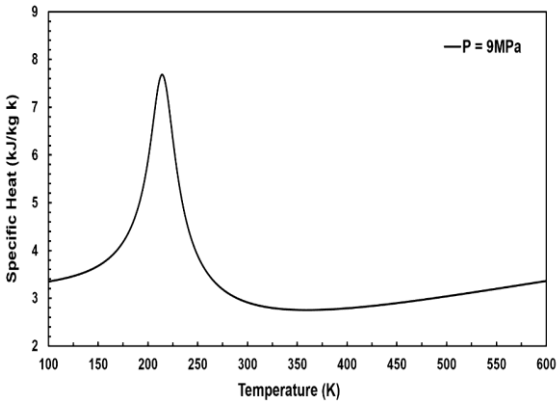

Fig. 1: Specific heat of Methane at a supercritical pressure

Our study investigates the heat transfer characteristics of supercritical methane in rectangular channels. It examines the influence of inlet velocities and channel aspect ratios on heat transfer efficiency and pressure losses.

2. Objectives

The objective of this research is to investigate the influence of inlet velocity and channel aspect ratio on heat transfer by forced convection using Methane as a coolant. The material used in this study is a copper alloy, with a width and height of 14 mm and 6 mm respectively, contains inside rectangular passage shape geometries with surface area A of 16 mm² with different aspect ratios height/width ("Rec-1" with an aspect ratio less than 1, "Rec-2" which is actually a square passage shape with an aspect ratio equal to 1 and finally "Rec-3" with an aspect ratio greater than 1). The length of the channels L is 300 mm which is generally equivalent to a combustion chamber length, heated on its lower surface. The internal wall thickness is 1 mm for each channel to ensure good heat transfer. Two 150 mm long fluid flow sections were added to allow for fully developed flow at the inlet and to avoid the effect of the boundary condition at the outlet. Due to symmetry, only half of the channel along the z-plane is used in the numerical calculation. The dimensions are illustrated in Fig. 2 and the boundary conditions in the Table 1.

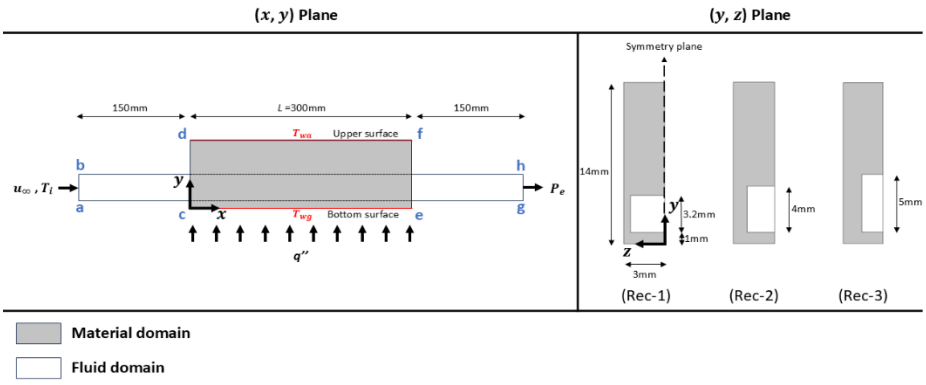

Fig. 2: Schematic view of the solution domain

Table 1: Boundary conditions.

Plans	Conditions
df	$\frac{\partial T}{\partial n} = 0$
ce	$\frac{\partial T}{\partial n} = q"\ 8\ \mathrm{MW/m^2}$
cd	$\frac{\partial T}{\partial n} = 0$

ef	$\frac{\partial T}{\partial n} = 0$
ab	$Ti = 120\text{K}$ u_∞ = 10, 15 and 20m/s
gh	Pe = 9MPa

This study fixes the inlet temperature Ti and the outlet pressure (operating pressure) Pe at 120 K and 9 MPa respectively, the constant heat fluxq'' is 8 MW/m², and inlet velocities u_∞ were varied from 5, 10, and 15m/s in the first part of the study and set to 10 m/s in the second part. Thermodynamic properties of methane are taken from the NIST database [13], and Copper's thermal conductivity from Simon et al. [14], integrated as Piecewise function. For this three-dimensional numerical study, the ANSYS-Fluent 18.1 software was used. Both fluid flow and heat transfer within the cooling channel are assumed to be stationary and turbulent. A tetrahedral mesh was applied to the entire domain (solid and fluid) with an element size of 4 × 10^-04 m. The resolution of the boundary layer near the walls was optimized using the Inflation in the meshing option. To meticulously capture the significant temperature gradient, especially near the wall region, the k-ε turbulence model with enhanced wall treatment is employed.

The equations governing continuity, momentum, and energy in the x, y, and z directions, which describe the flow and transport phenomena, are presented below [15] .

Continuity equation

$$\frac{\partial(\rho u_i)}{\partial x_i} = 0 \tag{1}$$

Momentum equation

$$\frac{\partial(\rho u_i)}{\partial \mathrm{t}} + \frac{\partial(\rho u_i u_j)}{\partial x_j} = -\frac{\partial \mathrm{P}}{\partial x_i} + \frac{\partial}{\partial x_j}\left[\mu\frac{\partial(u_i)}{\partial x_j} - \overline{\rho u'_\iota u'_\jmath}\right] \tag{2}$$

Energy equation

$$\frac{\partial}{\partial x_i}(\rho T) + \frac{\partial}{\partial x_i}(\rho u_i T) = \frac{\partial}{\partial x_i}\left[\frac{k}{C_p}\frac{\partial T}{\partial x_i}\right] \tag{3}$$

Transport equations in k-ε model

$$\frac{\partial}{\partial t}(\rho k) + \frac{\partial}{\partial x_i}(\rho k u_i) = \frac{\partial}{\partial x_j}\left[\left(\mu + \frac{\mu_t}{\sigma_k}\right)\frac{\partial k}{\partial x_j}\right] + G_k + G_b - \rho\varepsilon - Y_M + S_k \tag{4}$$

and

$$\frac{\partial}{\partial \mathrm{t}}(\rho\varepsilon) + \frac{\partial}{\partial x_i}(\rho\varepsilon u_i) = \frac{\partial}{\partial x_j}\left[\left(\mu + \frac{\mu_t}{\sigma_\varepsilon}\right)\frac{\partial \varepsilon}{\partial x_j}\right] + \rho\, C_1 S\varepsilon - \rho C_2 \frac{\varepsilon^2}{k + \sqrt{\nu\varepsilon}} + C_{1\varepsilon}\frac{\varepsilon}{k}C_{3\varepsilon}G_b + S_\varepsilon \tag{5}$$

where

$$C_1 = \max\left[0.43, \frac{\eta}{5+\eta}\right], \quad \eta = S\frac{k}{\varepsilon}, \quad S = \sqrt{2S_{ij}S_{ij}}$$

Turbulent viscosity

$$u_t = \rho\frac{k^2}{\varepsilon}\left[\frac{1}{4.04 + \sqrt{6}\frac{kU^*}{\varepsilon}\cos\varphi}\right] \tag{6}$$

where

$$U^* = \sqrt{S_{ij}S_{ij} + \acute{\Omega}_{ij}\acute{\Omega}_{ij}}, \quad \acute{\Omega}_{ij} = \Omega_{ij} - 2\varepsilon_{ijk}\omega_k, \quad \Omega_{ij} = \overline{\Omega_{ij}} - \varepsilon_{ijk}\omega_k, \quad \varphi = \frac{1}{3}\cos^{-1}\left(\sqrt{6}\Psi\right),$$

and

$$\Psi = \frac{S_{ij}S_{jk}S_{ki}}{\acute{S}^3}, \qquad \acute{S} = \sqrt{S_{ij}S_{ij}}, \qquad S_{ij} = \frac{1}{2}\left(\frac{\partial U_j}{\partial x_i} + \frac{\partial U_i}{\partial x_j}\right)$$

with

$C_{1\varepsilon} = 1.44, \qquad C_2 = 1.9, \qquad \sigma_k = 1.0, \qquad$ and $\sigma_\varepsilon = 1.2$

Note:

In Continuity, Momentum and Energy equations, ρ represents the fluid density, while u_i and u_j are the velocity component in the x, y and z axes. u_j denotes the velocity component in these directions. μ stands for the viscosity, and u' indicates the fluctuation in velocity, with $\overline{\rho u'_i u'_j}$ representing the turbulent stress. T is the temperature and P is the pressure. C_p is the specific heat, and k denotes thermal conductivity.

In transport equations, G_k corresponds to the generation of turbulence kinetic energy due to the mean velocity gradients, while G_b represents the generation of turbulence kinetic energy due to buoyancy, Y_M indicates the contribution of fluctuating dilatation in compressible turbulence to the overall dissipation rate.

Constants C_2 and $C_{1\varepsilon}$ are included. And σ_k and σ_ε are the turbulent Prandtl numbers for k and ε, respectively. S_k and S_ε are user-defined source terms.

In the turbulent viscosity expression, $\overline{\Omega_{ij}}$ is the mean rate of rotation tensor in a rotating reference frame with the angular velocity ω_k.

3. Results and discussion

3. 1. Effect of Different Inlet Velocities on Heat Transfer and Pressure Losses

This first part of the study examines the effect of inlet velocity on heat transfer performance and pressure losses. For this purpose, only the Rec-1 channel is used, with inlet velocities u_∞ set at 5, 10, and 15 m/s. The results, presented in Fig. 3, confirm that higher velocities significantly enhance heat transfer. For instance, a maximum difference of 118% in the heated wall temperature T_{wg} was observed between velocities of 5 and 15 m/s. However, this improvement comes with a substantial increase in pressure losses, as shown in Table 2. For example, for the same velocities of 5 and 15 m/s, a difference of 240% in pressure loss was recorded. These observations guide our study toward alternative solutions, such as those explored in the second part, where the channel aspect ratio is modified.

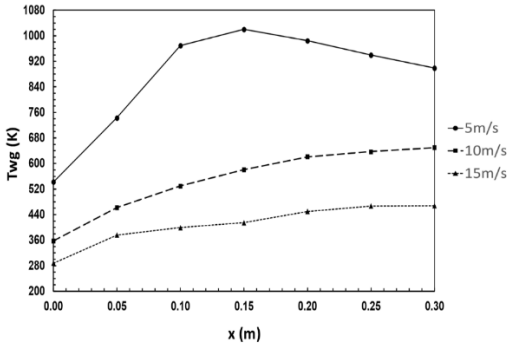

Fig. 3: Effect of different inlet velocities on heated wall temperature

Table 2: Pressure losses

	5m/s	10m/s	15m/s
ΔP (MPa)	0.015	0.026	0.051

Another phenomenon observed in this first study is the deterioration of heat transfer at 5 m/s. This is evidenced by a sudden rise in temperature over the first 0.15 m of the channel, followed by a decrease beyond this position. This phenomenon, widely studied [16], is attributed to differences in methane properties between "the region near the wall", where the temperature reaches the pseudo-critical point, where for example, the specific heat reaches a peak near this temperature (as seen in Fig. 1), and "the bulk region", where the temperature remains below this point. This creates a stratification effect between the two regions. Beyond 0.15 m, this effect diminishes as the property differences become less significant.

3. 2. Effect of Aspect Ratio

In this second part, the inlet velocity is fixed at 10 m/s, which yielded average results in terms of heat transfer and pressure losses in the first part. The objective is to evaluate the impact of channel aspect ratio on these parameters. The results shown in Fig. 4, Fig. 5 and Table 3 indicate that each channel has distinct advantages:

Aspect ratio < 1 (Rec-1): This channel records the lowest external (unheated) wall temperature T_{wg}. This feature is critical for next-generation rocket engines, which use thin external walls reinforced with composite overwrap. The T_{wa} temperature must remain within the operating limits of composite materials to prevent degradation.

Aspect ratio = 1 (Rec-2): This channel achieves the lowest pressure losses, although its wall temperatures, particularly T_{wa}, are slightly higher than those of Rec-1.

Aspect ratio > 1 (Rec-3): This channel significantly reduces the maximum heated wall temperature T_{wg} while maintaining moderate pressure losses. This configuration appears promising, offering a compelling trade-off compared to increasing velocities, which enhance heat transfer but result in very high-pressure losses.

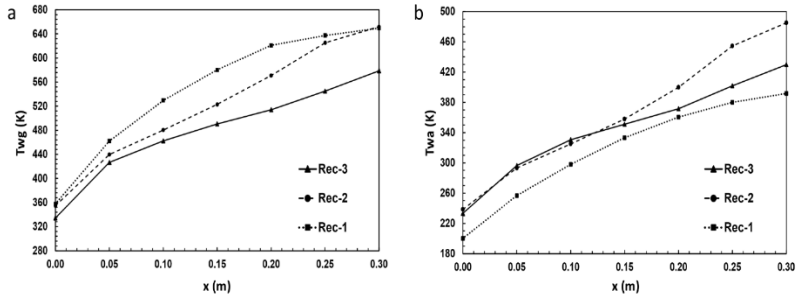

Fig. 4 : Variation of bottom wall temperature T_{wg} (a) and upper wall temperature T_{wa} (b)

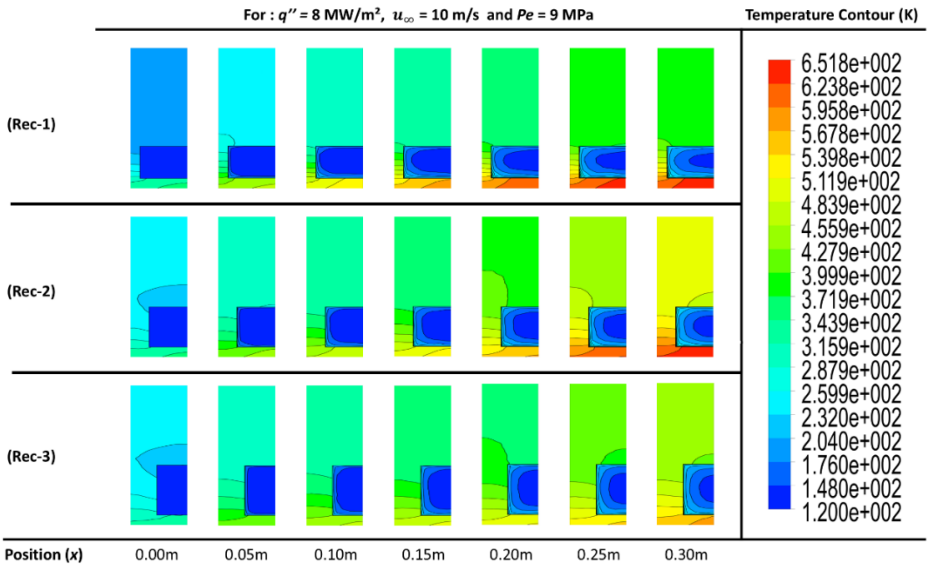

Fig. 5: Temperature distribution along the x-axis of each channel

Table 3: Aspect ratio effect on maximum wall temperatures T_{wg} and T_{wa}, and pressure losses

	Rec-1	Rec-2	Rec-3
Twg Max (K)	649.59	651.80	578.8
Twa Max (K)	391.54	485.19	429.74
ΔP (MPa)	0.026	0.025	0.028

4. Conclusion

This three-dimensional numerical study analyzed the effect of different inlet velocities and rectangular channel aspect ratios on heat transfer and pressure losses. The main findings are as follows:

Increasing inlet velocity significantly improves heat transfer but at the cost of high-pressure losses.

Modifying the channel aspect ratio influences wall temperatures (T_{wg} and T_{wa}) and pressure losses:

✓ Channels with an aspect ratio < 1 minimize T_{wa}, a critical feature for engines using reinforced composite materials.
✓ Channels with an aspect ratio = 1 minimize pressure losses.
✓ Channels with an aspect ratio > 1 reduce T_{wg} without a significant increase in pressure losses, providing a balanced solution.

These results pave the way for optimal configurations in regenerative cooling systems for rocket engines

Refrences

[1] N. Alili, K. Kaddouri, M. Salem, A. Alami, "Numerical Analysis of Convergent-Divergent Angles and Operating Conditions Impact on Rocket Nozzle Performance Parameters," INCAS BULLETIN, vol. 16, pp. 3–14, Mar. 2024. https://doi.org/10.13111/2066-8201.2024.16.1.1

[2] N. Alili, A. Benouar, M. A. Djeffal, K. Kaddouri, and M. Salem, "Novel Circular Arc Contour Design for Optimizing Rocket Nozzle Efficiency," Journal of Aeronautics, Astronautics and Aviation, vol. 56, no. 4, pp. 801–809, 2024. https://doi.org/https://doi.org/10.6125/JoAAA.202409_56(4).02

[3] D. S. Scannapieco, J. J. Lewandowski, R. B. Rogers, and D. L. Ellis, "In-Situ Alloying of GRCop-42 via Additive Manufacturing: Precipitate Analysis," 2020. https://ntrs.nasa.gov/citations/20205003857

[4] P. R. Gradl, C. Protz, J. Fikes, D. Ellis, L. Evans, A. Clark, S. Miller, T. Hudson, "Lightweight thrust chamber assemblies using multi-alloy additive manufacturing and composite overwrap," in AIAA Propulsion and Energy 2020 Forum, 2020, p. 3787. https://doi.org/https://doi.org/10.2514/6.2020-3787

[5] S. A. O'Briant, S. B. Gupta, and S. S. Vasu, "Laser ignition for aerospace propulsion," Propulsion and Power Research, vol. 5, no. 1, pp. 1–21, 2016. https://doi.org/https://doi.org/10.1016/j.jppr.2016.01.004

[6] T. Mundt, C. Knowlen, and M. Kurosaka, "Scale effects on rotating detonation rocket engine operation," Applications in Energy and Combustion Science, vol. 19, p. 100282, 2024. https://doi.org/https://doi.org/10.1016/j.jaecs.2024.100282

[7] M. A. Djeffal, N. Benamara, A. Lahcene, A. Benouar, A. Boulenouar, M. Merzoug, "Numerical Analysis of a Supercritical Heat Transfer of Cryogenic Methane in Regeneratively Cooled Rocket Engine," INCAS BULLETIN, vol. 16, no. 1, pp. 33–44, Mar. 2024. https://doi.org/10.13111/2066-8201.2024.16.1.4

[8] M. A. Djeffal, N. Benamara, A. Lahcene, N. Alili, K. Kaddouri, A. Benouar, A. Boulenouar, "Numerical Analysis of Supercritical Methane Heat Transfer in Regeneratively Cooled Liquid Propellant Rocket Engines," Journal of Aeronautics, Astronautics and Aviation, vol. 56, no. 4, pp. 835–844, 2024. https://doi.org/https://doi.org/10.6125/JoAAA.202409_56(4).05

[9] B. N. Bhat, "Aerospace Materials and Applications", Reston VA: American Institute of Aeronautics and

Astronautics, Inc., 2018. https://doi.org/10.2514/4.104893

[10] G. P. Sutton and O. Biblarz, Rocket propulsion elements. John Wiley & Sons, 2016. https://www.wiley.com/en-us/Rocket+Propulsion+Elements,+9th+Edition-p-9781118753910

[11] H. P. Trinh, "Liquid methane/oxygen injector study for potential future Mars ascent," in 36th AIAA/ASME/SAE/ASEE Joint Propulsion Conference and Exhibit, 2000, p. 3119. https://doi.org/10.2514/6.2000-3119

[12] M. K. and P. M. Thomas Brown, "Foundational Methane Propulsion Related Technology Efforts , and Challenges for Applications to Human Exploration Beyond Earth Orbit," Proceedings of Space Propulsion Conference 2016, no. May, 2016. https://doi.org/20160006972

[13] E. W. Lemmon, I. H. Bell, M. L. Huber, and M. O. McLinden, Thermophysical Properties of Fluid Systems", National Institute of Standards and Technology, 2023. https://webbook.nist.gov/chemistry/fluid/

[14] N. J. Simon, E. S. Drexler, R. P. Reed, R. M. White, and J. W. Lyons, "Properties of Copper and Copper Alloys at Cryogenic Temperatures Technology Admlnletndlon," NIST Monograph 177, 1992. https://nvlpubs.nist.gov/nistpubs/Legacy/MONO/nistmonograph177.pdf

[15] T.H. Shih, W.W. Liou, A. Shabbir, Z. Yang, J. Zhu, "A new k-ϵ eddy viscosity model for high reynolds number turbulent flows," Computers & fluids, vol. 24, no. 3, pp. 227–238, 1995. https://doi.org/10.1016/0045-7930(94)00032-T

[16] M. Pizzarelli, F. Nasuti , M. Onofri, P. Roncioni, R. Votta, F. Battista, "Heat transfer modeling for supercritical methane flowing in rocket engine cooling channels," Applied Thermal Engineering, 75, pp. 600-607, 2015. https://doi.org/10.1016/j.applthermaleng.2014.10.008